HiSST: 3rd International Conference on
High-Speed Vehicle Science & Technology

14–19 April 2024, Busan, Korea

Multi-Temperature Modelling of T4 Shock Tunnel Nozzle Flows

Robert Watt[1], Rowan Gollan[1], and Nicholas Gibbons[1]

Abstract

The thermal non-equilibrium state of the gas at the exit of shock tunnel nozzles can have a significant effect on the flow over the test article. The most common modeling of thermal non-equilibrium for hypersonic nozzle flows represents the non-equilibrium state using two temperatures: one for the translation and rotation; and one for the average vibrational energy of all the molecules. In this paper, we extend this model to account for a vibration temperature for each molecule, and compare to the more common approach of using two temperatures. Simulation of nozzle flows of conditions in the T4 shock tunnel facility was conducted using the extended multi-temperature model. It was found that the individual molecular vibration temperatures could vary from the two temperature model. For example, NO was found to relax significantly faster than N_2 and O_2 in all the conditions considered. The effect could be important for comparing against measurements of individual molecular temperatures, but the overall effect on the gas dynamics is small.

Keywords: *Non-equilibrium, Hypersonics*

Nomenclature

$\dot{\omega}$	Chemical source ($\mathrm{kg\,s^{-1}}$)	p	Pressure (Pa)
$\dot{Q}$	Energy source term ($\mathrm{J\,kg^{-1}\,s^{-1}}$)	q	Heat conduction vector
ρ	Density ($\mathrm{kg/m^3}$)	T_D	Characteristic dissociation temperature (K)
E	Total energy per unit mass ($\mathrm{J\,kg^{-1}}$)	u	Velocity ($\mathrm{m\,s^{-1}}$)

1. Introduction

Shock tunnels are one of the few methods for producing high-speed flows in a laboratory to study hypersonic vehicles, albeit only for a few milliseconds. Shock tunnels operate by expanding a slug of high-temperature and pressure gas through a converging-diverging nozzle, which then flows over the test article. By tuning the conditions of the slug of gas, and expanding it through an appropriate nozzle, flows replicating interesting high-speed flight conditions can be achieved.

The gas slug is often hot enough for the gas molecules to begin vibrating. As the gas cools in the nozzle, the molecules lose their vibrational energy through collisions. However, the expansion process may be so fast that the molecules do not undergo sufficient collisions to decrease their level of vibrational energy substantially, leaving them in a higher vibrational energy state as compared to equivalent flight conditions. In such a case, the gas is said to be in a frozen state of thermal non-equilibrium, as the vibration of the molecules appears to be frozen at a higher temperature relative to the translation temperature.

One fairly high-fidelity approach to predict the state of the gas exiting the nozzle is to use a Navier-Stokes simulation with thermochemical nonequilibrium effects. A common assumption is that the energy of the gas can be separated into two modes: one mode for the translational and rotational motion; and another for the vibration of all the molecules. The energy in each mode is assumed to follow a Boltzmann

[1] *School of Mechanical and Mining Engineering, Centre for Hypersonics, The University of Queensland, St. Lucia QLD 4072, Australia*

distribution, governed by a temperature unique to the mode. This gives two temperatures: T_{tr} is the *translation-rotation* temperature, and T_{vib} is the *average vibration* temperature. At thermal equilibrium, $T_{tr} = T_{vib}$.

Understanding the non-equilibrium state of the gas exiting the nozzle has proven to be important in analysing the flow over the test articles. For example, Nompelis et al. [1] found that not accounting for the non-equilibrium state at the nozzle exit led to a 20% over prediction of the heat transfer on a hypersonic double cone in a shock tunnel-produced test flow. Shen et al. [2, 3] use a two-temperature model developed by Park to account for thermal non-equilibrium effects in shock tunnel nozzles. They found that the importance of the non-equilibrium state varies from case to case. Separately, Gehre *et al* [4] found that although the vibration temperature at the nozzle exit was elevated, the total amount of energy in vibration was still low, and an equilibrium treatment of the nozzle was sufficient to model flow through a scramjet. In any case, predicting the impact of non-equilibrium is an important step in interpreting the results of shock tunnel campaigns.

Some diagnostic techniques have been used on shock tunnel nozzles to measure the vibration temperature of a specific molecule. However, the common two-temperature model does not indicate the amount of non-equilibrium between the vibration of different molecules. Therefore it is not clear that measurements of a particular molecular species are representative of the average vibration temperature across all molecules. Recent work from Caltech [5, 6] has measured the vibration temperature of NO behind a cylinder, which was found to be in equilibrium with translation, despite the two temperature model predicting non-equilibrium. Gross *et al* [6] argued a multi-temperature model would better predict the NO temperature since the two-temperature model is biased towards the abundant, but slowly relaxing N_2. Initial research into this discrepancy using the model developed here has proved promising.

In this paper, we extend the two temperature model to an arbitrary number of energy modes, allowing for a different vibration temperature for each molecule. This permits a more detailed exploration of the validity of the two temperature model for modeling shock tube nozzles. In particular, the validity of the two temperature model for modelling the nozzles of the University of Queensland's T4 shock tunnel will be evaluated. Section 2 outlines the governing equations and modeling of the source terms. Section 3 shows verification and validation of the new models, and section 4 presents simulations of T4 nozzles.

2. Governing Equations

The simulations in this paper will be performed using the hypersonic flow solver *Eilmer* [7], developed at the University of Queensland. Eilmer has been upgraded for this work to allow an arbitrary number of energy modes, allowing for one vibration temperature per molecule.

2.1. Governing equations

The compressible, chemically-reacting Navier-Stokes equations are solved, along with additional energy conservation equations to model the non-equilibrium distribution of energy. In the case of simulating modeled turbulence, the equations are augmented by additional equations for modeling turbulence in a Reynolds-averaged sense.

$$\frac{\partial \rho_s}{\partial t} + \frac{\partial}{\partial x_j}\left(\rho_s u_j\right) = \dot{\omega}_s \tag{1}$$

$$\frac{\partial}{\partial t}\left(\rho u_i\right) + \frac{\partial}{\partial x_j}\left(\rho u_i u_j\right) = -\frac{\partial p}{\partial x_j} + \frac{\partial \tau_{ij}}{\partial x_j} \tag{2}$$

$$\frac{\partial}{\partial t}\left(\rho E\right) + \frac{\partial}{\partial x_j}\left[\rho\left(E+p\right)u_j\right] = -\frac{\partial q_j}{\partial x_j} + \frac{\partial}{\partial x_j}\left(\tau_{ij}u_i\right) \tag{3}$$

$$\frac{\partial}{\partial t}\left(\rho e_n\right) + \frac{\partial}{\partial x_i}\left(\rho e_n u_i\right) = -\frac{\partial q_{i,n}}{\partial x_i} + \dot{Q}_{chem,n} + \dot{Q}_{V-T,n} + \dot{Q}_{V-V,n} \tag{4}$$

where ρ is total density of the gas, ρ_s is the partial density of species s, u_i is the bulk velocity in direction i, $\dot{\omega}_s$ is the chemical production source term for species s, p is the pressure of the gas, τ_{ij} is the viscous

stress tensor, E is the total energy of the gas, e_n is the energy stored in mode n, and q_i is the total heat conduction in direction i, and $q_{i,n}$ is the heat conduction of mode n in direction i. The equations of state to close eqs. (1) to (4) are presented in section 2.2, while the chemical and energy exchange source terms, $\dot{\omega}_s$, $\dot{Q}_{chem,n}$, $\dot{Q}_{V-T,n}$, and $\dot{Q}_{V-V,n}$ are described in sections 2.3 and 2.4.

2.2. Thermodynamics

The total energy of the gas has contributions from each of the energy modes. Each energy mode is assumed to follow a Boltzmann distribution, at its own unique temperature.

$$E = e_{tr} + \sum_{n=1}^{N} e_n \tag{5}$$

where e_n is the energy in mode n, and N is the total number of energy modes modelled. e_n may have contributions from the vibration of molecules or electronic excitation:

$$e_n = \sum_i e_{i,n} \tag{6}$$

where i represents the i^{th} energy mode contributing to mode n. For example, mode $n = 1$ could have contributions from N_2 vibration ($i = 0$) and N_2 electronic excitation ($i = 1$).

The translational/rotational energy of species s is computed assuming this mode is fully excited

$$e_{tr,s} = c_{v,s}(T_{tr} - T_{ref}) + e_s^\circ \tag{7}$$

where $c_{v,s}$ is the specific heat at constant volume of species s. e_s° is the formation energy of species s evaluated at the reference temperature (T_{ref}). This is computed from the thermodynamic curve fits of McBride ***et al*** [8].

The electronic energy is calculated via the partition function

$$e_{e,s}(T_{e,s}) = R_s \frac{\sum_i g_i^s \theta_{e,i}^s \exp\left(-\theta_{e,i}^s / T_{e,s}\right)}{\sum_i g_i^s \exp\left(-\theta_{e,i}^s / T_{e,s}\right)} \tag{8}$$

where $T_{e,s}$ is the temperature governing the electronic excitation of species s, $\theta_{e,i}^s$ is the characteristic temperature of the i^{th} electronic excitation state of species s, and g_i^s is the degeneracy of the i^{th} electronic excitation state of species s.

The vibrational energy of each species is calculated using the thermodynamic curve fits from McBride ***et al*** [8], subtracting off the electronic and translation components.

$$e_{vib,s} = e_s(T_{vib,s}) - e_{e,s}(T_{vib,s}) - e_{tr,s}(T_{vib,s}) \tag{9}$$

where $T_{vib,s}$ is the temperature governing the vibrational excitation of species s.

The mixture energy is computed using a mass fraction weighted sum of the contribution from each species

$$e_n = \sum_s Y_s e_{n,s} \tag{10}$$

where $e_{n,s}$ is the energy of species s in mode n, and Y_s is the mass fraction of species s, in an approach similar to that described in Gnoffo [9].

2.3. Chemical rates

The chemical source terms appearing in eq. (1), $\dot{\omega}_s$, have contributions from all the reactions being modeled, which involve species s. In general, a chemical reaction is represented as

$$\sum_{s=1}^{N} \alpha_s X_s \longleftrightarrow \sum_{s=1}^{N} \beta_s X_s \tag{11}$$

where α_i and β_i are the stoichiometric coefficients of the reactants and products. For this reaction, the mass production rate of species s is given by

$$\frac{\mathrm{d}[X_s]}{\mathrm{d}t} = (\beta_s - \alpha_s)\left(k_f \prod_i [X_i]^{\alpha_i} - k_b \prod_i [X_i]^{\beta_i}\right) \tag{12}$$

where k_f and k_b are the forward and backward rate constants respectively, $[X_i]$ is the concentration of species i, and i represents each species taking part in the reaction. Estimating k_f and k_b forms the basis of the modeling of chemical reactions, and can be done with varying levels of sophistication, and varying levels of coupling with thermal non-equilibrium.

The work-horse chemical reaction rate model is the *Arrhenius* model. The Arrhenius model curve fits the rate constant to the translation-rotation temperature of the gas and does not account for any non-equilibrium effects.

$$k_{arr}\left(T_{tr}\right) = A T_{tr}^{n} \exp\left(-\frac{C}{T_{tr}}\right) \tag{13}$$

where A, C, and n are model parameters.

The Arrhenius model can be modified to account for non-equilibrium effects with various approaches. One such approach is the *Marrone-Treanor* model. In the Marrone-Treanor model, the forward rate constant is the product of the Arrhenius rate constant and a non-equilibrium correction factor

$$k_f\left(T_{tr}, T_{v,i}\right) = k_{arr}\left(T_{tr}\right) Z\left(T_{tr}, T_{v,i}\right) \tag{14}$$

$$Z\left(T_{tr}, T_{v,i}\right) = \frac{Q\left(T_{tr}\right) Q\left(T_F\right)}{Q\left(T_{v,i}\right) Q\left(-U\right)} \tag{15}$$

Q is an approximation to the vibrational partition function, U is a model parameter describing how preferential the dissociation is, and T_F is a pseudo-temperature

$$Q\left(T\right) = \frac{1 - \exp\left(-T_D/T\right)}{1 - \exp\left(-\theta_v/T\right)} \tag{16}$$

$$\frac{1}{T_F} = \frac{1}{T_{v,i}} - \frac{1}{T_{tr}} - \frac{1}{U} \tag{17}$$

The *Modified-Marrone-Treanor* model introduces a temperature dependence on U

$$\frac{1}{U} = \frac{a_U}{T_{tr}} + \frac{1}{U^\star} \tag{18}$$

where a_U and $U^\star$ are now the model parameters.

Each dissociation removes some energy from the vibration energy of the dissociating molecule,

$$-\frac{\epsilon_{vib}}{k_B} = \frac{\theta_{vib}}{\exp\left(\theta_{vib} T_F\right)} - \frac{T_D}{\exp\left(T_D/T_F\right)} \tag{19}$$

In this work, the Modified-Marrone-Treanor model is used, with parameters from [10].

2.4. Energy exchange rates

2.4.1. Vibration-translation exchanges

Vibration-translation energy exchanges occur when a molecule collides with another molecule or atom and leaves the collision in a different vibrational energy state. This energy exchange type is denoted V-T. V-T energy exchanges are modeled using the Landau-Teller model:

$$\dot{Q}_{V-T,s} = \sum_j \frac{e_s^\star - e_s}{\tau_{sj}} \tag{20}$$

where $e_s^\star$ is the vibrational energy of species s at equilibrium with the translation/rotation temperature, and $\tau_{s,j}$ is the relaxation time. The relaxation time can be approximated using various models, including Millikan-White [11], and a recent model developed by Torres *et al* [10].

2.4.2. *Vibration-vibration exchanges*

A vibration-vibration energy exchange occurs when two molecules collide, one molecule exits the collision in a higher vibrational energy state, and the other leaves the collision in a lower vibration energy state. This type of energy exchange is denoted V-V. To model separate vibration temperatures, the energy exchanges between the vibrational modes of two molecules colliding need to be accounted for. A model for the rate of this energy exchange was proposed by Thivet *et al* [12]

$$\dot{Q}_{V-V,s} = \sum_{q=0,q\neq p}^{n_{vib}-1} \frac{x_q}{\tau_{V-V}^{p-q}} \left(\frac{1-\exp\left(-\theta_{vib,p}/T\right)}{1-\exp\left(-\theta_{vib,q}/T\right)} \frac{e_{vib,q}}{\hat{e}_{vib,q}} \left(\bar{e}_{vib,p} - e_{vib,p}\right) - \frac{e_{vib,p}}{\hat{e}_{vib,q}} \left(\bar{e}_{vib,q} - e_{vib,q}\right) \right) \tag{21}$$

where $\bar{e}_{vib,p}$ is the vibration energy, assuming a truncated harmonic oscillator, of species p, evaluated at equilibrium with the translation/rotation temperature. Similarly, $\hat{e}_{vib,p}$ is the vibration energy, assuming a harmonic oscillator, of species p, evaluated at equilibrium with the translation/rotation temperature.

The thermal relaxation time, τ_{V-V}^{p-q}, can be approximated using an extension by Thivet *et al* [12] to the theory developed by Schwartz, Slawsky and Herzfeld [13]. The theory assumes colinear collisions, rotationless molecules, and mono-quantum transitions. The relaxation time is given by:

$$\tau_{V-V}^{pq} = \left[Z_{coll}^{p-q} P_{01}^{10}\left(A_p, A_q\right) \right]^{-1} \exp\left(-\left(\theta_v^p - \theta_v^q\right)/T\right) \tag{22}$$

Here, Z_{coll}^{pq} is the collision frequency, and P_{01}^{10} is the probability of a vibrational energy exchange happening for each collision, and θ_v^p is the characteristic (first excited state) vibration temperature of species p. The transition probability can be approximated as

$$P_{ij}^{kl}\left(A_p, A_q\right) = \frac{\mathcal{A}}{Z_0^p Z_0^q Z_V^p Z_V^q Z_T^{pq} Z_+^{pq}} \tag{23}$$

where each Z is a steric factor, and $\mathcal{A}$ is the collision cross-reference factor,

$$\mathcal{A} = \left(r_{pq}^{c\star}/\sigma_{pq}\right)^2 \tag{24}$$

The orientation steric factors are given by

$$Z_0^p = \left[\delta_{pq}^{\star} r_p + \frac{5}{2} \left(1/\left(\delta_{pq}^{\star} r_p\right)^2 \right) \right]^{-1} \tag{25}$$

where r_p is the interatomic distance of molecule p in the ground vibration state. The vibration steric factors are derived assuming only mono-quantum transitions

$$Z_V^p = \frac{f_m^p}{(i+1)\,\pi^2} \frac{\mu_{pp}}{\mu_{pq}} \frac{\alpha_{pq}}{\theta_v^p} \left(\frac{k_B \theta_v^p}{\Delta E} \right)^2 \tag{26}$$

where

$$f_m^p = \left(m_p \bar{C_p^2}\right)^{-1} \tag{27}$$

$$\bar{C_p^2} = \frac{m_X^2 + m_Y^2}{2 m_X m_Y \left(m_X + m_Y\right)} \tag{28}$$

where X and Y represent the atoms forming molecule p. The translation steric factor is given by

$$Z_T^{pq} = \pi^2 \left(\frac{3}{2\pi} \right)^{1/2} \left(\frac{\Delta E}{k_B \alpha_{pq}} \right)^2 \left(\frac{T}{\alpha_{pq}} \right)^{1/6} \exp\left[\frac{3}{2} \left(\frac{\alpha_{pq}}{T} \right)^{1/3} - \frac{\Delta E}{2 k_B T} \right] \tag{29}$$

Finally, the steric factor dealing with attractive forces is given by

$$Z_+^{pq} = \exp\left[-\frac{4}{\pi} \left(\frac{\epsilon_{pq}^0 \chi_{pq}^{\star}}{k_B T} \right)^{1/2} - \frac{16}{3\pi^2} \frac{\epsilon_{pq}^0}{k_B T} \right] \tag{30}$$

The remaining quantities are:

$$\alpha_{pq} = \frac{16\pi^4 \mu_{pq} \Delta E^2}{(\delta^\star_{pq})^2 h^2 k_B} \tag{31}$$

$$\chi^\star_{pq} = \frac{1}{2}\left(\frac{\alpha_{pq}}{T}\right)^{1/3} \tag{32}$$

$$\delta^\star_{pq} r^0_{pq} = \frac{12}{(2\beta)^{1/6}}\left(1 + \frac{21}{19}\beta\right) \tag{33}$$

$$\frac{r^0_{pq}}{r^{c\star}_{pq}} = \frac{1}{(2\beta)^{1/6}}\left(1 + \frac{2}{19}\beta\right) \tag{34}$$

$$\beta = \left[\frac{1}{2}\left(\frac{2\epsilon^0_{pq}}{\mu_{pq}}\right)^9 \left(\frac{3h\mu_{pq}}{\pi^2 r^0_{pq} k_B T \Delta E}\right)^6\right]^{1/19} \tag{35}$$

3. Verification and Validation

Verification and validation of the current implementation of the multi-temperature model is presented in this section. Verification of the vibration-vibration energy exchanges is performed in section 3.1, and two validation cases are presented in section 3.2 and section 3.3.

3.1. Post shock relaxation

To verify the vibration-vibration energy exchanges have been implemented correctly, the relaxation of non-reacting air behind a shock wave was compared to results obtained by Thivet ***et al*** [12], see fig. 1. The vibration-vibration exchanges are computed as per section 2.4.2. The vibration-translation energy exchanges were computed using the Landau-Teller model, with a relaxation time based on the same extended SSH theory as the vibration-vibration relaxation time. Excellent agreement is achieved with Thivet ***et al*** [12], providing confidence the current implementation of V-V exchanges is correct. However, this does not validate the V-V exchange model, as no experimental data is available for this case. Sections 3.2 and 3.3 provide some comparisons with experiments to validate the V-V exchanges.

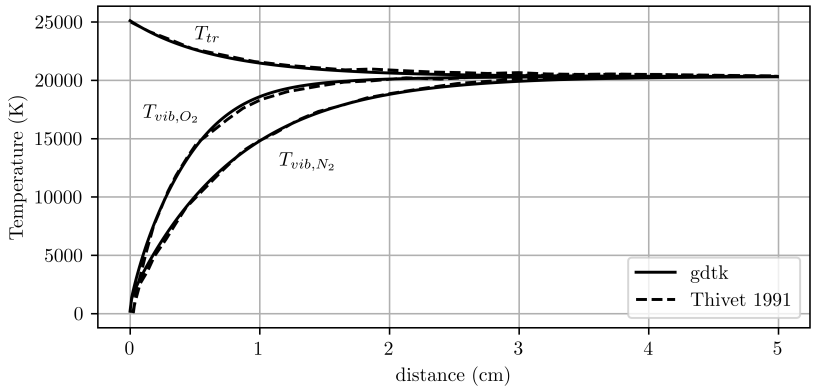

Fig 1. Comparison of post-shock relaxation of air behind a normal shock ($X_{O_2} = 0.21$, $X_{N_2} = 0.79$, $u_\infty = 7.175\,\text{km/sec}$, $T_\infty = 205\,\text{K}$, $p_\infty = 2.5\,\text{Pa}$)

3.2. Low Enthalpy Expansion: Univeristy of Virginia Supersonic Combustion Facility

Cutler ***et al*** [14] measured the vibration temperature of N_2 and O_2 in The University of Virginia Supersonic Combustion Facility (UVaSCF) using dual-pump CARs. These measurements can be used to validate the current multi-temperature model. The facility pre-heats air to $1200\,\text{K}$ before expanding it to approximately Mach 2 through a converging-diverging nozzle, followed by a constant area test section.

The enthalpy of the flow is approximately $1\,\mathrm{MJ\,kg^{-1}}$, which is lower than what T4 is capable of producing (recalling simulations of T4 are the goal of this work). The vibration temperature of N_2 and O_2 were measured at the end of the constant area test section. A schematic of the simulation domain is shown in fig. 2. Further geometry and flow conditions details can be found in [14].

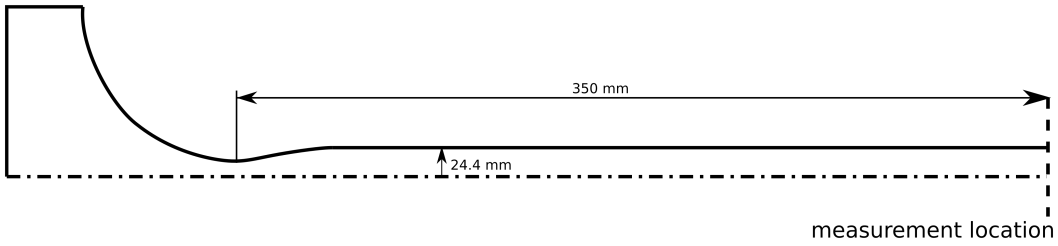

Fig 2. Computational domain for UVaSCF simulations

The inflow was modeled as a stagnation region ($p = 296\,\mathrm{kPa}$, $T = 1200\,\mathrm{K}$) at thermochemical equilibrium, which was isentropically expanded to the velocity just inside the domain. The flow was assumed to be fully turbulent with the Spalart-Allmaras-Edwards model [15]. Given the low temperature of the flow, the flow was chemically non-reactive, and therefore no chemistry modeling was used. A two-species gas model (N_2 and O_2) was used to model the thermodynamics. The flow was hot enough in the nozzle supply region for vibrational excitation, and the expansion was fast enough for vibrational freezing. Therefore, the multi-temperature model was used, where N_2 and O_2 each had their own vibration temperature. The electronic excitation of each molecule was assumed equilibrated with that molecule's vibration temperature. The vibration-translation energy exchanges were modeled using the QCT rates derived by Torres *et al* [10]. Figure 3a shows the temperatures at the measurement location without V-V exchanges, while fig. 3b includes V-V exchanges. Good agreement is observed without V-V exchanges, however their presence causes the N_2 temperature to drop too low. One possible reason for the poor agreement with V-V exchanges is the assumptions made by the extended SSH theory used to develop the relaxation time fall apart at the low temperatures present in this flow. Section 3.3 provides a validation case, at a higher enthalpy condition, including vibration-vibration exchanges.

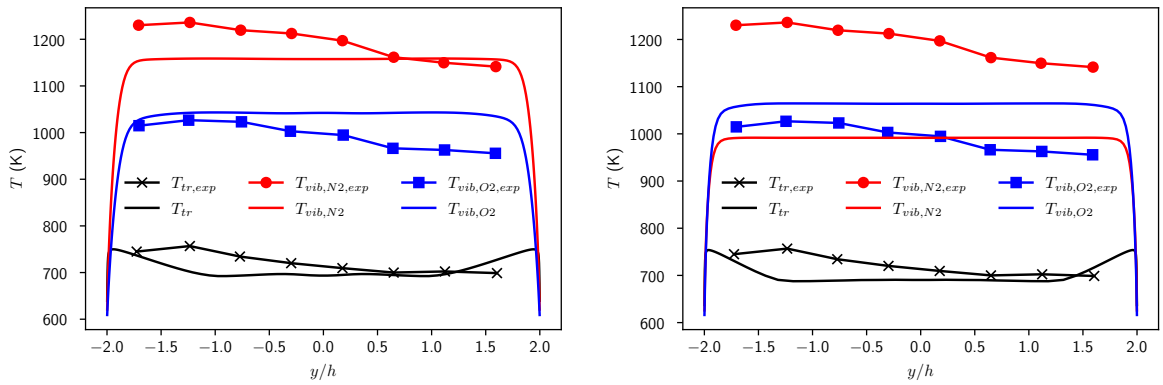

(a) Without V-V exchanges

(b) With V-V exchanges

Fig 3. Comparison of measured and simulated N_2 and O_2 vibration temperatures in the UVaSCF facility

3.3. High Enthalpy Expansion: DLR L3K Facility

Another validation test, conducted to exercise the vibration-vibration energy exchanges in a region where they are likely more reliable, is the DLR L3K arc-jet tests performed by Gülhan *et al* [16]. The test flow

in this case had an enthalpy of $8.4\,\mathrm{MJ\,kg^{-1}}$, which is a realistic enthalpy for T4.

The L3K facility was simulated using a seven-species air gas model (N_2, O_2, NO, N, O, NO^+, e^-), with each neutral molecule having a unique vibration temperature. The NO^+ vibration temperature and free-electron translation temperature were assumed to be in equilibrium with the vibration temperature of N_2. The chemistry model from Gupta *et al* [17] was used, and Millikan-White [11] vibration-translation relaxation times were used for better consistency with the numerics in [16]. A comparison of the simulated Nitrogen vibration temperature, with and without V-V exchanges, and the experimental measurements is shown in fig. 4a. Including V-V exchanges drastically improves the agreement between the measured and simulated Nitrogen vibration temperatures, providing confidence in the V-V exchange model, and bringing the model mostly in line with the two-temperature model.

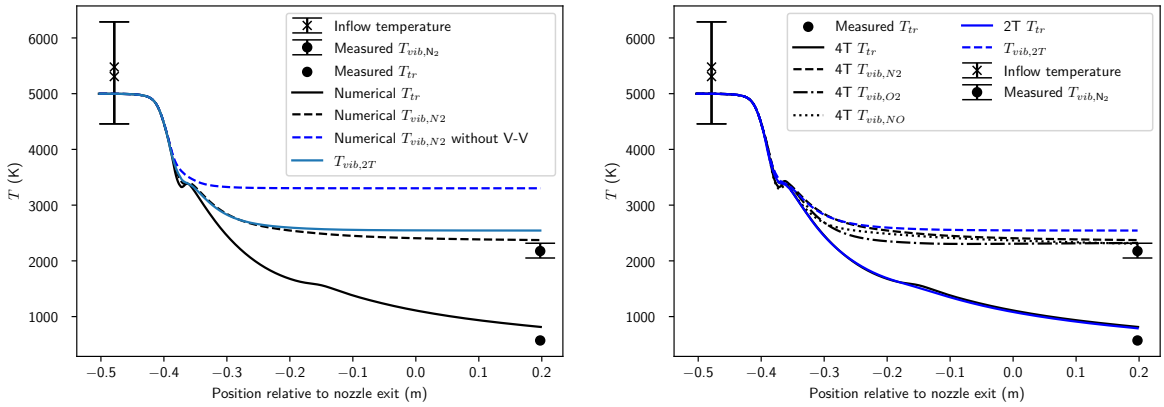

(a) Comparison with and without V-V exchanges

(b) All temperatures

Fig 4. Temperatures along the centre line of L3K facility

Only the N_2 vibration temperature was measured, meaning validation of the V-V exchanges for the other molecules was not possible. However, since the model for V-V exchanges relies on the fundamental properties of the molecules, rather than fitting experimental data, accurately predicting $T_{v,\mathrm{N_2}}$ provides confidence in the theoretical model. This confidence extends to the other molecules. Naturally, more experimental data of the other vibration temperatures would be preferable, but this data is seldom measured.

3.4. Comments on validation

The validation presented here gives some confidence in the thermodynamic models used in the multi-temperature model, and in the chemical and kinetics modeling under appropriate flow conditions. However, more experimental measurements of individual molecular vibration temperatures would be valuable for validating the models. In particular, the vibration-vibration energy exchanges need further validation at temperatures present in T4, and possibly alternative (or improved) models for low temperatures. Based on the results obtained here, the vibration-vibration exchanges seem to not be reliable at low temperatures, while at temperatures obtainable in T4, it seems to be reasonable.

4. Non-equilibrium simulations of T4 nozzle flows

A comparison of the two-temperature and multi-temperature model in the Univeristy of Queensland's reflected shock tunnel, T4, is presented here.

4.1. Simulation setup

The simulations performed here consist only of the diverging part of the nozzle. A five species chemically reacting gas model was used (N_2, O_2, N, O, NO) to model the thermodynamics. The Modified-Marrone-Treanor model was used for the chemistry source terms, and the V-T relaxation time of Torres [10] was used. The vibration-vibration exchanges were modeled using the theory outlined in section 2.4.2. The

conditions at the nozzle throat are estimated from the stagnation region by isentropically expanding the stagnation state to Mach 1. Table 1 summarises the stagnation conditions considered. The gas in the stagnation region is assumed to be in thermochemical equilibrium.

Condition	h (MJ kg^{-1})	T (K)	p (MPa)	Mach number	Shot number	Reference
B	2.89	2663	12.6	7	12409	[18]
C	7.61	5292	88.6	10	11985	[19]

Table 1. Summary of conditions in nozzle reservoir

A description of the Mach 7 nozzle contour can be found in Chan ***et al*** [20], and a description of the Mach 10 nozzle can be found in Towsey [21]. Since the nozzles are axisymmetric, the simulations are two-dimensional, with axisymmetric source terms added. The base grid is 150×25 cells, clustered at the wall, see fig. 5. The flow was assumed fully turbulent, transitioning 0.1 m from the nozzle throat for the Mach 7 nozzle, and 0.15 m from the throat for the Mach 10 nozzle. Chan ***et al*** [20] found the location of transition varying from 0.05 m to 0.15 m for this nozzle did not significantly affect the numerical estimate of the flow generated by the Mach 7 nozzle. The Spalart-Allmaras-Edwards model [15] was used to model the turbulence. The simulations were conducted using Eilmer's steady-state solver, which uses the Jacobian-free Newton-Krylov method [22].

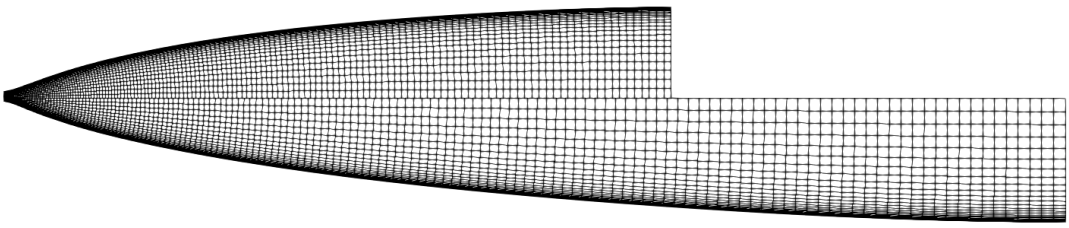

Fig 5. Base computational grid. Top: Mach 7 nozzle, Bottom: Mach 10 nozzle.

4.2. Grid and iterative convergence

A grid convergence study was conducted to ensure the results presented were properly resolved. The four grid resolutions used are 150×25, 300×50, 450×150, and 550×200. Figure 6 plots the errors in the various modeled temperatures (relative to the finest grid) at the centre of the nozzle exit plane, for the two conditions. It is clear that all the simulations there is negligible change between the two finest grids, giving confidence in grid converged solutions. All simulations presented in the remainder of this section are for the finest grid. All simulations converged at least 8 orders of magnitude in the relative global residual.

4.3. Results and discussion

Figure 7a shows the temperatures along the centre-line of the nozzle for condition B. All the temperatures predicted by the multi-temperature model for this case are lower than the average vibration temperature predicted by the two-temperature model. This is because the extra degrees of freedom can change the path the gas takes to equilibrium. For example, allowing different vibration temperatures can change the dissociation/recombination rate for that molecule, thus changing the composition of the gas. Another way the extra non-equilibrium can alter the state is by different thermal relaxation rates. For example, N_2 is allowed to relax much faster due to V-T exchanges, which will decrease the total vibrational energy content of the flow. The lower NO temperature causes N_2 and O_2 to relax faster due to V-V exchanges with NO. Since V-V exchanges are generally not resonant due to the different quantum vibration energy levels of the different molecules, the V-V exchanges also modify the total vibration energy content of the flow, rather than just moving the temperatures closer to equilibrium with one another. This is potentially

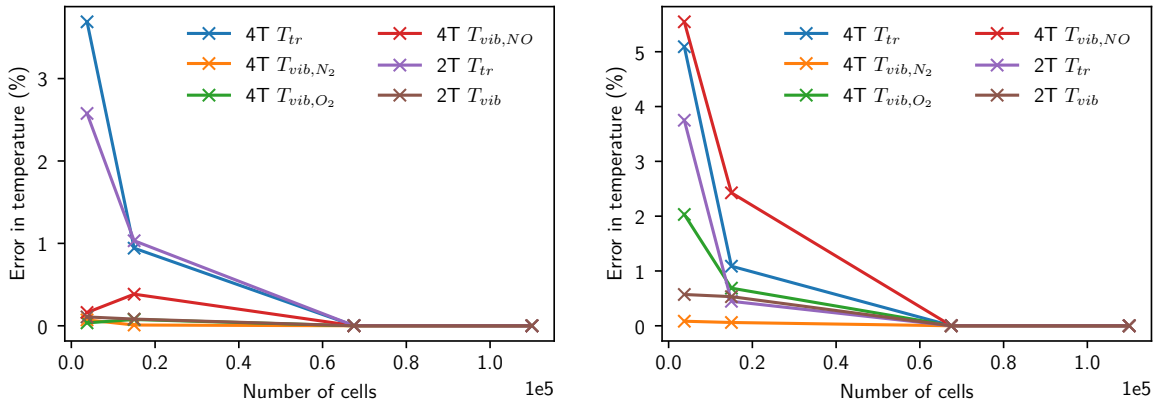

(a) Condition B **(b)** Condition C

Fig 6. Grid convergence

exaggerated by the modeling defect noted in the UVaSCF simulations, although the temperatures in condition B are higher than in UVaSCF. The translation-rotation temperatures predicted by both models were indistinguishable, indicating the difference in vibrational energy content of the flow is minimal.

Figure 7b shows the temperatures along the centre line of the nozzle for condition C, which is a flow condition with comparable enthalpy to the L3K validation case. In this condition, the two-temperature model predicted only a little non-equilibrium, while the multi-temperature model predicted freezing of $T_{v,\mathrm{N_2}}$. In the multi-temperature model, the vibration temperature of NO is in equilibrium with the translation/rotation temperature, and O_2 is almost in equilibrium at the exit of the nozzle. The translation temperature did not change an appreciable amount.

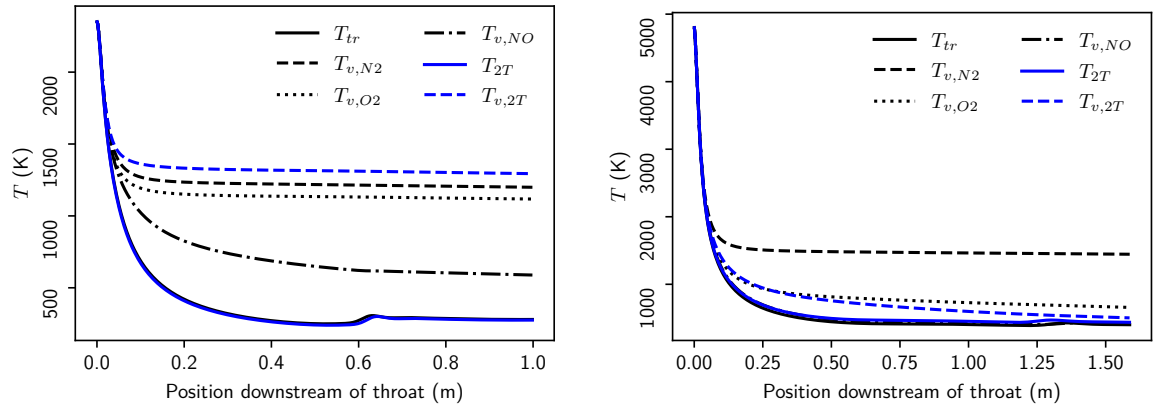

(a) Condition B **(b)** Condition C

Fig 7. Temperatures along the nozzle centre-line

In both cases, it is clear that measuring the vibration temperature of an arbitrary molecule, and assuming this is representative of the average vibration temperature, would lead to erroneous conclusions about the vibrational state of the gas exiting the nozzle. However, the two-temperature model reasonably predicts the average vibrational energy of the flow, even though it does not give any indication of the distribution of the vibration energy amongst the molecules. Therefore, the need for a multi-temperature

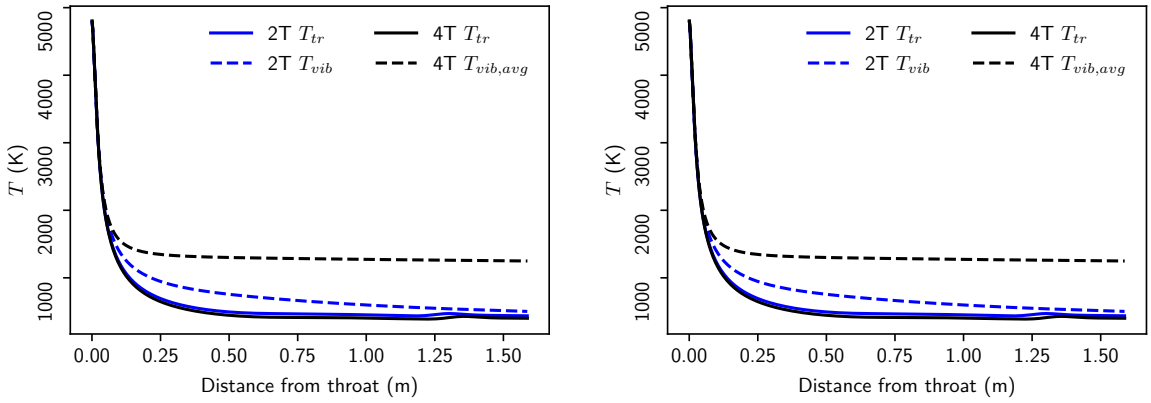

(a) Condition B **(b)** Condition C

Fig 8. Comparison of the average of the 4T model with 2T model temperatures along the nozzle centre-line

model to model shock tube nozzles largely comes down to the intent of the simulation. If only an idea of the vibrational energy content of the flow is required, the two-temperature model will suffice. However, the multi-temperature model will likely provide a better comparison to experimental measurements of individual molecular vibration temperatures.

Figure 9 compares the ratio of specific heats, $\gamma = {}^{C_p}/_{C_v}$, along the centre-line of the nozzle, as a proxy for the effect on the gas dynamics. For the low enthalpy case, the change in γ is negligible. In the high enthalpy case, the γ value at the nozzle exit is reduced by approximately 4–5% in the multi-temperature model compared to the two-temperature model. This is due to N_2 freezing in the multi-temperature model. The effect on the translation temperature is not noticed since most of the expansion happens with the gas in equilibrium. Further, the effect of the change in γ is likely not a measurable effect on the gas dynamics of the flow over the test article, given other larger uncertainties in shock tunnel operation. Therefore, the overall gas dynamics are not significantly affected by the extra non-equilibrium degrees of freedom.

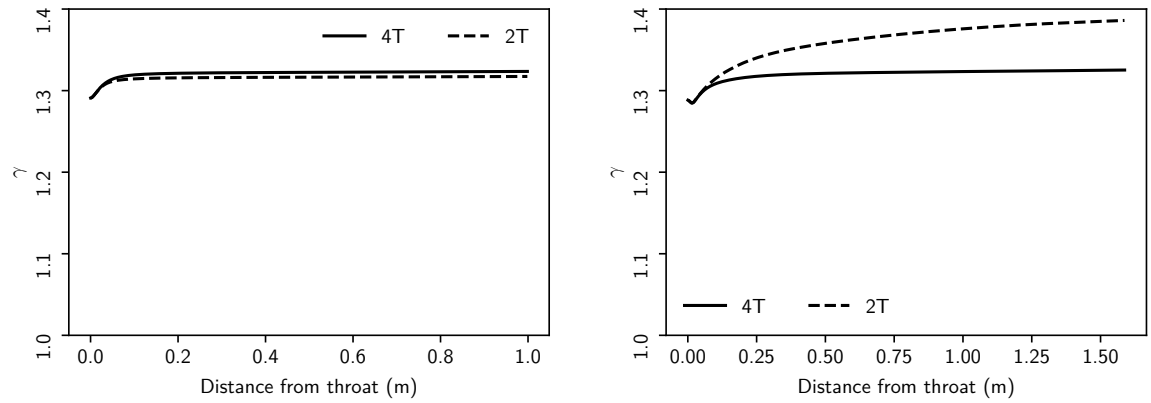

(a) Condition B **(b)** Condition C

Fig 9. Comparison of γ along the nozzle centre-line

5. Conclusions

A multi-temperature model was implemented in the hypersonic flow solver, Eilmer, to investigate the validity of the two-temperature model. In particular, the non-equilibrium in the T4 shock tunnel at the Univeristy of Queensland was investigated. While more experimental data of individual molecular vibration temperatures is required for thorough validation, reasonable agreement was observed in flows with similar enthalpies to T4 shots. The model for energy exchanges between vibrational modes was observed to over-predict the relaxation rate of Nitrogen at low enthalpies but was not observed at higher enthalpies. One possible reason for this is the assumptions of the theoretical model the relaxation time are based upon falls apart at low temperatures. Further work to improve the relaxation time estimates at these low temperatures would be beneficial.

Simulations of a Mach 7 and Mach 10 shot of T4 were conducted. It was found that Nitrogen generally relaxed slower than predicted by the two-temperature model, while NO relaxed faster. If measurements of individual molecular vibration temperatures are performed, a multi-temperature treatment of the flow may be required to compare the experimental and simulated temperatures. In the high-enthalpy shot, the multi-temperature model reduced the γ value by approximately 4–5% compared to the two-temperature model. This change in γ is likely not an experimentally measurable effect, and the overall gas dynamics are not significantly affected.

References

[1] I. Nompelis, G. V. Candler, and M. S. Holden, “Effect of vibrational nonequilibrium on hypersonic double-cone experiments,” *AIAA Journal*, vol. 41, pp. 2162–2169, 2003.

[2] J. Shen, H. Lu, R. Li, X. Chen, and H. Ma, “The thermochemical non-equilibrium scale effects of the high enthalpy nozzle,” *Advances in Aerodynamics*, vol. 2, 12 2020.

[3] J. Shen, Z. Shao, F. Ji, X. Chen, H. Lu, and H. Ma, “High enthalpy non-equilibrium expansion effects in turbulent flow of the conical nozzle,” *Aerospace*, vol. 10, 5 2023.

[4] R. M. Gehre, V. Wheatley, and R. R. Boyce, “Computational investigation of thermal nonequilibrium effects in scramjet geometries,” *Journal of Propulsion and Power*, vol. 29, pp. 648–660, 2013.

[5] J. J. Girard, P. M. Finch, T. Schwartz, C. L. Strand, R. K. Hanson, W. M. Yu, J. M. Austin, and H. G. Hornung, “Characterization of the T5 reflected shock tunnel freestream temperature, velocity, and composition using laser absorption spectroscopy,” American Institute of Aeronautics and Astronautics Inc, AIAA, 2021.

[6] T. J. Gross, E. Torres, T. E. Schwartzentruber, P. M. Finch, J. J. Girard, T. Schwartz, Z. N. Granowitz, C. L. Strand, R. K. Hanson, W. M. Yu, J. M. Austin, and H. G. Hornung, “Simulations of non-equilibrium air chemistry compared to hypersonic wind tunnel experiments,” 2024.

[7] N. N. Gibbons, K. A. Damm, and P. A. Jacobs, “Eilmer: An open-source multi-physics hypersonic flow solver,” *Computer Physics Communications*, vol. 282, p. 108551, 2023.

[8] B. J. McBride, M. J. Zehe, and S. Gordon, “NASA Glenn coefficients for calculating thermodynamic properties of individual species,” Tech. Rep. 211556, NASA, 2002.

[9] P. A. Gnoffo, R. N. Gupta, J. L. Shinn, and D. C. Washington, “Conservation equations and physical models for hypersonic air flows in thermal and chemical nonequilibrium,” 1989.

[10] E. Torres, T. Gross, and T. E. Schwartzentruber, “Implementation of new multi-temperature nonequilibrium air chemistry model for cfd based on first-principles calculations,” in *AIAA AVIATION 2023 Forum*, no. 2023-3489, 2023.

[11] R. C. Millikan and D. R. White, “Systematics of vibrational relaxation,” *The Journal of Chemical Physics*, vol. 39, pp. 3209–3213, 1963.

[12] F. Thivet, M. Y. Perrin, and S. Candel, “A unified nonequilibrium model for hypersonic flows,” *Physics of Fluids A*, vol. 3, pp. 2799–2812, 1991.

[13] R. N. Schwartz, Z. I. Slawsky, and K. F. Herzfeld, “Calculation of vibrational relaxation times in gases,” *The Journal of Chemical Physics*, vol. 20, pp. 1591–1599, 1952.

[14] A. D. Cutler, G. Magnotti, L. M. L. Cantu, E. C. A. Gallo, P. M. Danehy, R. Baurle, R. Rockwell, C. Goyne, and J. Mcdaniel, “Measurement of vibrational non-equilibrium in a supersonic freestream using dual-pump cars,” 2012.

[15] J. R. Edwards and S. Chandra, “Comparison of eddy viscosity-transport turbulence models for three-dimensional, shock-separated flowfields,” 1996.

[16] A. Gülhan, B. Esser, U. Koch, M. Fischer, E. Magens, and V. Hannemann, “Characterization of high-enthalpy-flow environment for ablation material tests using advanced diagnostics,” *AIAA Journal*, vol. 56, pp. 1072–1084, 2018.

[17] R. N. Gupta, J. M. Yos, and R. A. Thompson, “A review of reaction rates and thermodynamic and transport properties for 11-species air model for chemical and thermal non-equilibrium calculations to 30000k,” 1989.

[18] C. Eric, “Hypersonic shock impingement studies on a flat plate with elevated wall temperatures,” 2021.

[19] L. Will, “Improving performance of high mach number scramjets: Fuelling strategies and combustor design,” 2018.

[20] W. Chan, M. Smart, and P. Jacobs, “Flowpath design of an axisymmetric mach 7.0 nozzle for T4,” 2013.

[21] D. Towsey, “Design and optimisation of a mach 10 expansion nozzle,” 2004.

[22] K. A. Damm, N. N. Gibbons, P. A. Jacobs, and R. Gollan, “Application of a jacobian-free newton-krylov method to the simulation of hypersonic flows,” American Institute of Aeronautics and Astronautics (AIAA), 1 2023.